Lithos 364–365 (2020) 105485

Contents lists available at ScienceDirect

Lithos

journal homepage: www.elsevier.com/locate/lithos

Research article

Geochronology and geochemistry of the fossil-flora-bearing Wuda Tuff in North China Craton and its tectonic implications

Man Wang [a,b], Yu-ting Zhong [a], Bin He [a,*], Steven W. Denyszyn [c], Jun Wang [d,b], Yi-gang Xu [a,b,e]

[a] State Key Laboratory of Isotope Geochemistry, Guangzhou Institute of Geochemistry, Chinese Academy of Sciences, Guangzhou 510640, China
[b] College of Earth and Planetary Sciences, University of Chinese Academy of Sciences, Beijing 100049, China
[c] School of Earth Science, University of Western Australia, Perth WA6009, Australia
[d] State Key Laboratory of Palaeobiology and Stratigraphy, Nanjing Institute of Geology and Palaeontology, Center for Excellence in Life and Paleoenvironment, Chinese Academy of Sciences, Nanjing 210008, China
[e] Institutions of Earth Sciences, Chinese Academy of Sciences, Beijing 100029, China

ARTICLE INFO

Article history:
Received 25 October 2019
Received in revised form 29 February 2020
Accepted 12 March 2020
Available online 17 March 2020

Keywords:
Wuda vegetational Pompeii
Altered tuff
North China Craton
Zircon U—Pb geochronology
Geochemistry
Alxa Terrane

ABSTRACT

The Wuda Tuff Flora in the North China Craton (NCC) is a "vegetational Pompeii" and one of the most completely preserved marsh ecosystems of the late Paleozoic Northern Hemisphere. However, the precise age, geochemistry, and petrogenesis of the thick tuff containing this peat-forming flora have not been established. We conducted a comprehensive petrographic, mineralogical, whole-rock geochemical, and zircon U—Pb and Hf—O isotopic investigation of five samples from a vertical section through the tuff bed. Our results confirm that the material that buried the flora is a volcanic tuff bed that has undergone intensive post-deposition alteration. Whole-rock Al_2O_3/TiO_2 ratios (65.8–103.5) and negative Eu/Eu* values (0.27–0.38) further suggest a felsic volcanic origin. Secondary ion mass spectrometry zircon U—Pb dating of the altered tuff bed yielded a weighted mean $^{206}Pb/^{238}U$ age of 295.9 ± 1.4 Ma (1σ, MSWD = 0.94, n = 39), constraining the age of the Wuda Tuff Flora to the earliest Permian. Depletions of Nb and Ta in both the whole-rock and zircon compositions indicate an arc-related setting for the volcanism. The positive εHf(t) values (0.0 to +5.0) and $\delta^{18}O$ values (5.05‰–6.17‰) of zircon grains from the Wuda Tuff suggest a juvenile crust origin of the volcanic magma. Geochemical comparisons with contemporaneous igneous rocks suggest that the volcanic eruption that led to the formation of the Wuda Tuff and associated vegetational Pompeii was most probably caused by arc volcanism along the western margin of the NCC related to subduction of Paleo-Asian Ocean oceanic crust, implying that the Alxa Terrane had not yet amalgamated with the NCC during the early Permian.

1. Introduction

The Wuda Tuff Flora in the Wuda Coalfield in the North China Craton (NCC) is known as a "vegetational Pompeii" on account of its *in situ* high-quality preservation of plant remains (Wang et al., 2012), and estimates of its age range from latest Carboniferous to late early Permian (*e.g.*, Sun and Deng, 2003; Wang and Pfefferkorn, 2013). Besides important discoveries of some new taxa, such as *Paratingia wudensis* (Wang et al., 2009), *Aphlebia hvistendahliae* (Wang et al., 2014a), *Chansitheca wudaensis* (He et al., 2016), and *Scolecopteris libera* (Li et al., 2019), the Wuda Tuff Flora represents a rare reconstructed paleoecosystem based on actual sites of plant fossil communities (Wang et al., 2012). Therefore, the tuff flora provides valuable information for understanding the evolution of forest biological communities during the Permian. Numerous plant identifications and quantitative analyses have demonstrated that the Wuda Tuff Flora differs from the known typical NCC floral assemblages at that time, although it shows both similarities and differences compared with contemporaneous floras in Europe and North America (*e.g.*, Wang, 2010; Wang and Pfefferkorn, 2013). Although comprehensive studies of the paleobotany and paleoecology of the Wuda Flora have been conducted (*e.g.*, Wang et al., 2014b; Yan et al., 2013; Zhou et al., 2019), no detailed investigation of the tuff bed containing these fossil plants has been performed.

Characterizing the Wuda Tuff is crucial to a better understanding of the vegetational Pompeii formation. Wang et al. (2012) suggested that the Wuda Tuff Flora was preserved in volcanic ash, but no solid petrographic, mineralogical, or geochemical evidence was provided to support that conclusion. Moreover, an early Permian age for the Wuda Tuff Flora has been deduced from biostratigraphic correlations but has not yet been confirmed by geochronology (*e.g.*, Sun et al., 1998; Sun and Deng, 2003; Wang and Pfefferkorn, 2013). If it could be confirmed that the Wuda Tuff Flora is preserved in a volcanic tuff, direct dating of this tuff would provide a precise age for the flora, and knowledge of

* Corresponding author.
E-mail address: hebin@gig.ac.cn (B. He).

https://doi.org/10.1016/j.lithos.2020.105485
0024-4937/

the geochemical characteristics of the tuff would improve understanding for the formation mechanism of the vegetational Pompeii. Furthermore, the Wuda Tuff is located near the boundary of the NCC and the Alxa Terrane (ALT). The timing of collision between the NCC and the ALT is still uncertain owing to overprinting by strong intraplate deformation (Dan et al., 2016; Darby and Ritts, 2002; Yuan and Yang, 2015a, 2015b; Zhang et al., 2013). However, pyroclastic deposits near the plate boundary would likely have originated from volcanism caused by plate convergence. Thus, the Wuda Tuff may record the NCC–ALT collision event and thereby help clarify the tectonic evolution of this region.

For this study, we collected five rock samples from the bed containing the Wuda Tuff Flora, examined their petrography, mineralogy, and whole-rock geochemistry, and conducted secondary ion mass spectrometry (SIMS) zircon U—Pb and Hf—O isotopic analyses of zircons from the samples. On the basis of the results, we establish that the bed yielding the Wuda Tuff Flora is indeed a volcanic tuff layer. We present the formation age of the tuff and discuss the formation mechanism of the vegetational Pompeii. We also provide tectonic implications for the surrounding region on the basis of the geochronology and geochemistry of the Wuda Tuff.

2. Geological background and sampling

The NCC is bounded by the Central Asian Orogenic Belt (CAOB) to the north, the Sulu orogenic belt to the east, and the Qinling–Dabie orogenic belt to the south (Fig. 1a). A Carboniferous–Permian continental magmatic arc developed at the northern margin of the NCC as a result of subduction of Paleo-Asian Ocean (PAO) crust, which gave rise to the E–W-trending tectonic unit of the Inner Mongolia Paleo–Uplift (IMPU; Li, 2006; Zhang et al., 2007a). During the middle late Carboniferous, a large-scale northward transgression occurred, meaning that the paleogeographical units of the NCC during the late Carboniferous to early Permian ranged successively from north to south as uplands, alluvial–fluvial plains, paralic deltas, tidal flats (or tidal flat–barrier complexes), to shallow-marine environments (Liu, 1990). The corresponding deposits (Taiyuan Formation) comprise sandstones, limestones, shales and coals, and local conglomerates (Liu, 1990). Moreover, continuing plate subduction and frequent volcanism along the margin of the NCC led to the formation of widely distributed pyroclastic deposits now preserved in Carboniferous to Permian coal seams (Wang et al., 2016; Zhang et al., 2007b).

The Wuda Coalfield is located at the northwestern margin of the Helan Mountain Range and the western margin of the NCC near the boundary with the ALT (Fig. 1a). The Wuda Tuff Flora covers an area of about 20 km^2 (39°28′48″N to 39°33′36″N, 106°36′36″E to 106°39′36″E) and lies within a syncline (Figs. 1b–c, 2a; Wang et al., 2012). Stratigraphically, the Wuda Tuff Flora occurs in the uppermost part of the Taiyuan Formation between coal beds Nos. 6 and 7 (Fig. 1c; Wang et al., 2012), which were formed in a peat-forming environment in an alluvial plain setting (Dai et al., 2002, 2015). In the studied section (39°32′25″N, 106°38′02″E), the bed yielding the Wuda Tuff Flora is 66 cm thick. Five bulk samples were collected vertically throughout the section, designated as WD-8 to WD-12 from bottom to top (Fig. 1c).

3. Analytical techniques

3.1. Zircon SIMS U—Pb geochronology and in situ Hf—O isotopic analyses

Zircon crystals were purified by hand-picking under a binocular microscope after applying standard heavy liquid and magnetic separation techniques. Transmitted- and reflected-light photomicrographs and cathodoluminescence (CL) images were taken to define the structures of zircons and choose potential sites for U—Pb dating and Hf isotopic analyses. CL images were obtained using a Carl Zeiss SUPRA55SAPPHIR field emission SEM + Gatan MonoCL4 instrument at the SKLIG, GIGCAS.

Zircon SIMS U—Pb analyses were conducted using a CAMECA IMS1280-HR system at the SKLIG, GIGCAS, following a similar analytical procedure to that described by Li et al. (2009). The spot size of the ion beam was about 20 μm × 30 μm. The zircon standard Plešovice (337.13 Ma; Slama et al., 2008) was analyzed once every four unknowns to calibrate Pb/U ratios based on the linear relationship between ln ($^{206}Pb/^{238}U$) and $ln(^{238}U^{16}O_2/^{238}U)$ (Whitehouse et al., 1997). The standard Qinghu (Li et al., 2013) was analyzed as a secondary standard. Eight analytical spots of Qinghu yielded a concordia age of 159.6 ± 1.7 Ma, identical to the recommended value (159.5 ± 0.2 Ma, 2σ). Data reduction was performed using the Isoplot/Ex 3 software (Ludwig, 2003).

Zircon O isotopic analyses were performed *in situ* using the same CAMECA IMS1280-HR SIMS at GIGCAS, following the analytical procedures described by Li et al. (2010a). The $^{133}Cs^+$ primary ion beam with an intensity of ~2 nA was accelerated at 10 kV, and the diameter of analytical spots was about 20 μm (10 μm beam diameter + 10 μm raster). The zircon standard Penglai ($\delta^{18}O_{VSMOW}$ = 5.3‰, Li et al., 2010b) was analyzed once every four unknowns to correct for instrumental mass fractionation. The internal precision of the $^{18}O/^{16}O$ ratio for a single analysis was generally better than 0.1‰ (1σ). The external precision measured by the Penglai standard was 0.30‰ (2σ, n = 24). The Qinghu zircon standard yielded a weighted mean $\delta^{18}O$ = 5.4‰ ± 0.22‰ (2σ, n = 19), identical to the reported value of 5.4‰ ± 0.2‰ (Li et al., 2013).

Zircon *in situ* Hf isotopic analyses were conducted using a Neptune Plus MC–ICP–MS instrument (Thermo Scientific), coupled with a RESOlution M-50193 nm laser ablation (LA) system (Resonetics) at GIGCAS. A detailed description of the two instruments can be found in Zhang et al. (2014). The data reduction procedure followed Zhang et al. (2015). Twenty-two analyses of Plešovice zircon yielded a weighted mean $^{176}Hf/^{177}Hf$ = 0.282478 ± 0.000011 (2σ), consistent with the value reported by Slama et al. (2008).

3.2. Zircon trace-element analysis

Zircon trace-element compositions were measured using LA–ICP–MS at the facility of Wuhan Sample Solution Analytical Technology, Wuhan, China. Laser sampling was performed using a GeoLas ProHD LA system. An Agilent 7700e ICP–MS instrument was used to acquire ion-signal intensities following the operating procedure and conditions reported by Liu et al. (2008). A spot size of 32 μm and a laser frequency of 5 Hz were used for analyses during this study. Glass NIST610 was used as an external standard for trace-element calibration. Each analysis incorporated a background acquisition of approximately 20–30 s followed by 50 s of data acquisition. Data reduction and analysis were conducted using the Excel-based software ICPMSDataCal (Liu et al., 2008).

3.3. Mineralogical and whole-rock geochemical analyses

All samples were powdered to ~200-mesh size (≤74 μm) for geochemical analysis. Powder X-ray diffraction (XRD; Bruker D8 Advance) was used to determine whole-rock mineral compositions at the Key Laboratory of Mineralogy and Metallogeny, Guangzhou Institute of Geochemistry, Chinese Academy of Sciences (GIGCAS), Guangzhou, China. The operating conditions were a voltage of 40 kV, a current of 30 mA, a 2θ interval of 3°–85°, a slit width of 1 mm, and a scanning speed of 4/min. Specific analytical procedures followed those described by Hou et al. (2017).

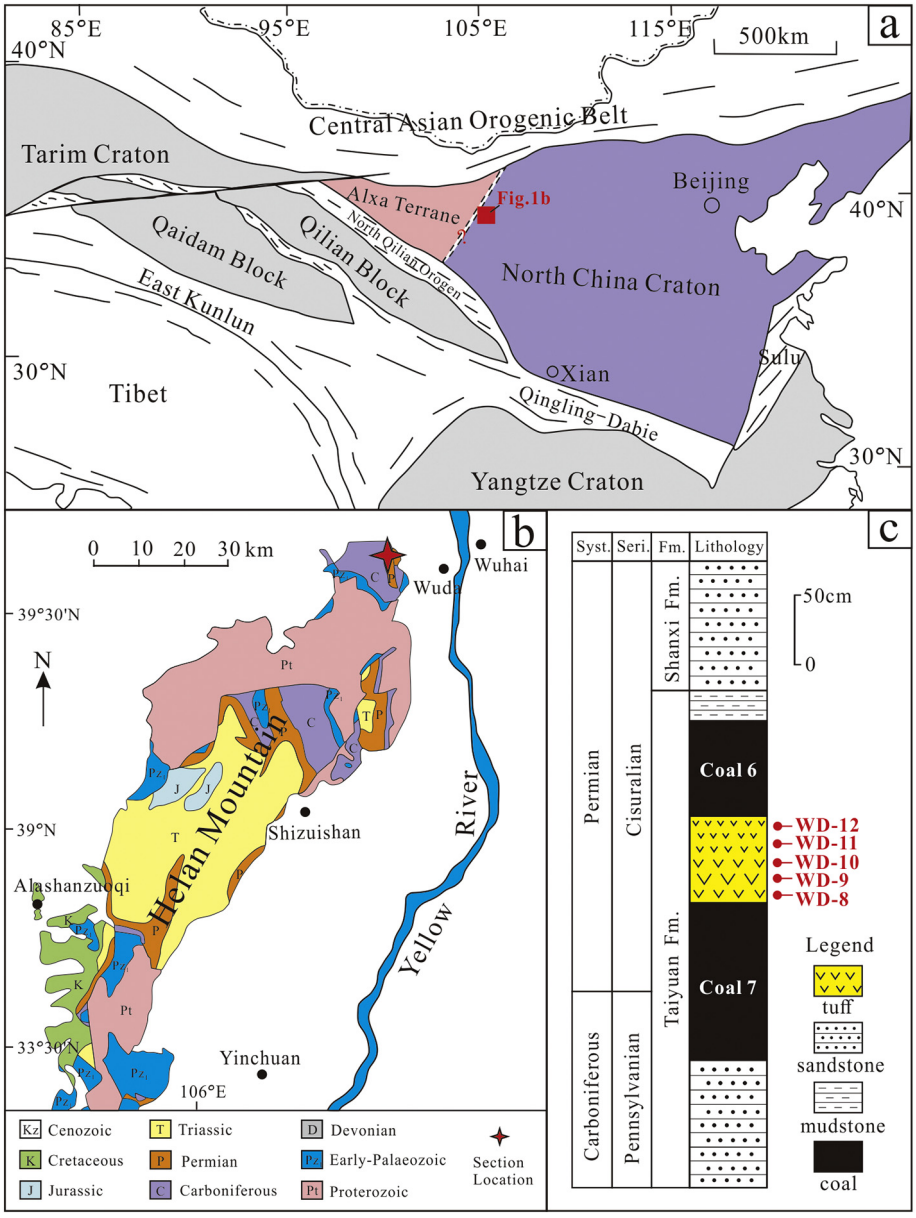

Fig. 1. (a) Tectonic sketch map of the NCC and adjacent regions, showing the location of the studied area. Modified after Dan et al. (2016). (b) Geological map of the Helan Mountain Range and the location of the Wuda section. (c) Stratigraphic column and sampling locations of the Wuda Tuff from Wuda Coalfield, North China.

Scanning electron microscopy (SEM) combined with energy-dispersive X-ray spectroscopy (EDS) was conducted on polished thin-sections of the samples for petrographic analysis, including the identification of mineral occurrence modes. Major-oxides analyses of whole rocks were performed using X-ray fluorescence spectrometry (XRF) on fused glass disks using a Rigaku ZSX-100e XRF instrument at the State Key Laboratory of Isotope Geochemistry (SKLIG), GIGCAS. Pre-ignition was used to determine the loss on ignition (LOI) prior to major-element analyses. Analytical procedures followed those presented by Goto and Tatsumi (1996). Quantitative calibration was performed using data from 36 reference materials (Li et al., 2005). The precision of major-element contents is less than 1%. Trace-element contents were determined using an Agilent 7500a inductively coupled plasma–mass spectrometry (ICP–MS) instrument at GIGCAS, following the techniques described by Li et al. (2000). Detailed digestion procedures can be found in the supplementary files. Rock standards including BHVO-2, GSR-1, GSR-2, GSR-3, AGV-2, GSR-10, W-2, and SARM-4 were used for calibration. The precision of trace element analyses is <5%.

4. Results

4.1. Petrography and mineralogy

The samples are gray to dark-gray claystones and are dense and hard with conchoidal fracture planes. Irregular laminations defined by plant fragments are observed (Fig. 2a). All samples are matrix-supported by cryptocrystalline kaolinite and are composed of authigenic kaolinite crystals, pyroclastic crystal fragments, and organic detritus, as observed under polarized optical microscopy (Fig. 2b, c). Authigenic kaolinite occurs as vermicular aggregates, plate-like or angular brecciated fragments, or infillings or replacements of plant fragments. Pyroclastic crystal fragments are mainly quartz, feldspar, and minor biotite, with grain sizes between 0.02 and 0.4 mm. Quartz fragments show classical volcanogenic textures of angular shapes and corrosion gulfs (Fig. 2b, c). SEM–EDS analyses indicate that most feldspar fragments preserve their original plate-like shapes but have been altered to kaolinite (Fig. 2d).

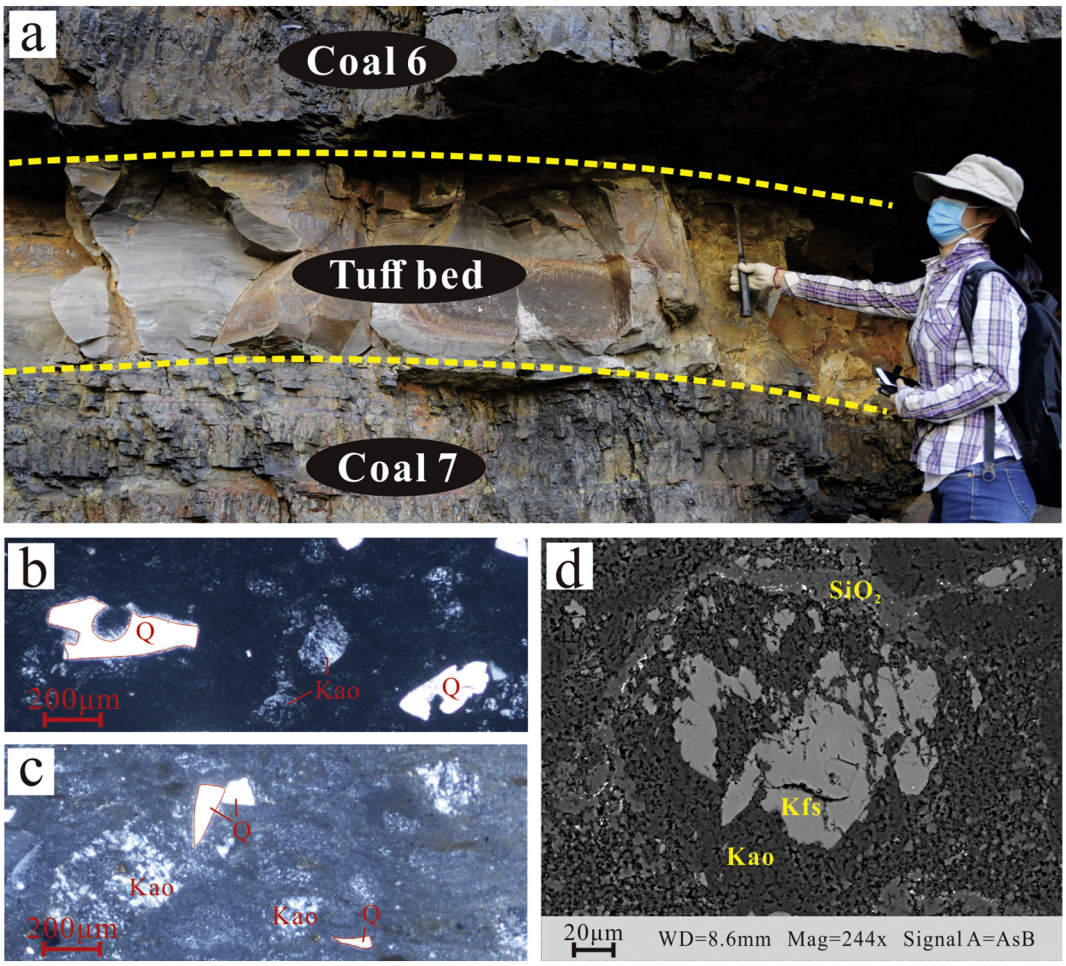

Fig. 2. (a) Field photograph of the Wuda Tuff bed. (b) Photomicrograph of sample WD-8, showing corrosion gulfs of quartz grains. (c) Photomicrograph of sample WD-9, showing angular quartz grains. (d) SEM image showing alteration structure from K-feldspar to cryptocrystalline kaolinite. Abbreviations: Q: quartz; Kao: kaolinite; Kfs: K-feldspar.

Color and grain-size differences through the Wuda bed profile allow the three parts to be distinguished (Figs. 1c and 2a); a lower part (sample WD-8), a middle part (sample WD-9), and an upper part (samples WD-10, WD-11, and WD-12). Organic contents in the lower and upper parts are higher than those of the middle part, as reflected in their darker color. Plant fragments and kaolinite crystals in the middle part are coarser than those in the lower and upper parts.

Results of XRD analysis (Supplementary Table S1) are consistent with polarized optical microscope observations of thin-sections. As the XRD results show, the samples are composed of kaolinite (74.3%–86.5%) and quartz (10.7%–25.7%) with minor K-feldspar. Of the samples, WD-10 has the lowest kaolinite (78.3%) and highest quartz (25.7%) contents and WD-11 has the highest kaolinite (86.5%) and lowest quartz (10.7%) contents.

4.2. Major and trace elements

Results of major-element analyses are given in Supplementary Table S1. LOI values range from 10.6 to 13.4 wt%. The analyzed samples have high SiO_2 (50.7–57.0 wt%) and Al_2O_3 (30.0–33.6 wt%), and low K_2O (0.49–0.92 wt%), Na_2O (<0.1 wt%), CaO (<0.05 wt%), and MgO (0.31–0.37 wt%) contents. P_2O_5 contents range from 0.03 to 0.04 wt%, and MnO contents are negligible. Fe_2O_3 contents vary from 0.23 to 0.68 wt% and TiO_2 from 0.30 to 0.47 wt%. Al_2O_3/TiO_2 ratios lie between 65.8 and 103.5. Values of the chemical index of alteration (CIA, Nesbitt and Young, 1982) that used to measure the degree of chemical weathering, range from 96.7 to 98.1.

Results of trace-element analyses are given in Supplementary Table S1. Contents of Cr and Mn increase gradually upward through the profile from sample WD-8 to WD-12, whereas U contents decrease. Sample WD-11 has the highest Sc (9.76 ppm), Ti (3091 ppm), V (23.68 ppm), and Ga (39.06 ppm) contents.

The total rare earth element (ΣREE) contents of the Wuda samples vary from 124.1 ppm (WD-11) to 467.0 ppm (WD-9). Loss of REEs may have occurred during chemical reaction of the upper and lower parts of the tuff layer with the overlying and underlying coal seams. The element Y displays a similar pattern to that of the REEs (Fig. 3a, b). Previous studies have reported that some elements normally regarded as immobile (*e.g.*, Y, Th, Nb, and REEs) may be mobile in coal seams (Dai et al., 2016; Hower et al., 1999). In the Chondrite-normalized REE diagrams, all of the studied samples show enrichment in light REEs [$(La/Yb)_{CN} = 10.3–16.7$] and negative Eu anomalies ($Eu/Eu^* = 0.27–0.38$; Fig. 3a). Variable levels of depletion in Nb, Ta, and Ti are observed in a primitive-mantle-normalized trace-element spidergram (Fig. 3b).

4.3. Zircon U—Pb geochronology

Samples WD-9 and WD-10 were selected for zircon U—Pb geochronological analyses (Supplementary Table S2). Most of the zircon grains are clear, euhedral to subhedral, and 20–200 μm long, with aspect ratios of 1:1 to 5:1. The analyzed zircons show oscillatory magmatic zoning in CL images (Fig. 4) and have Th/U ratios of >0.3. These features suggest that the zircons are magmatic in origin (Hoskin and Schaltegger,

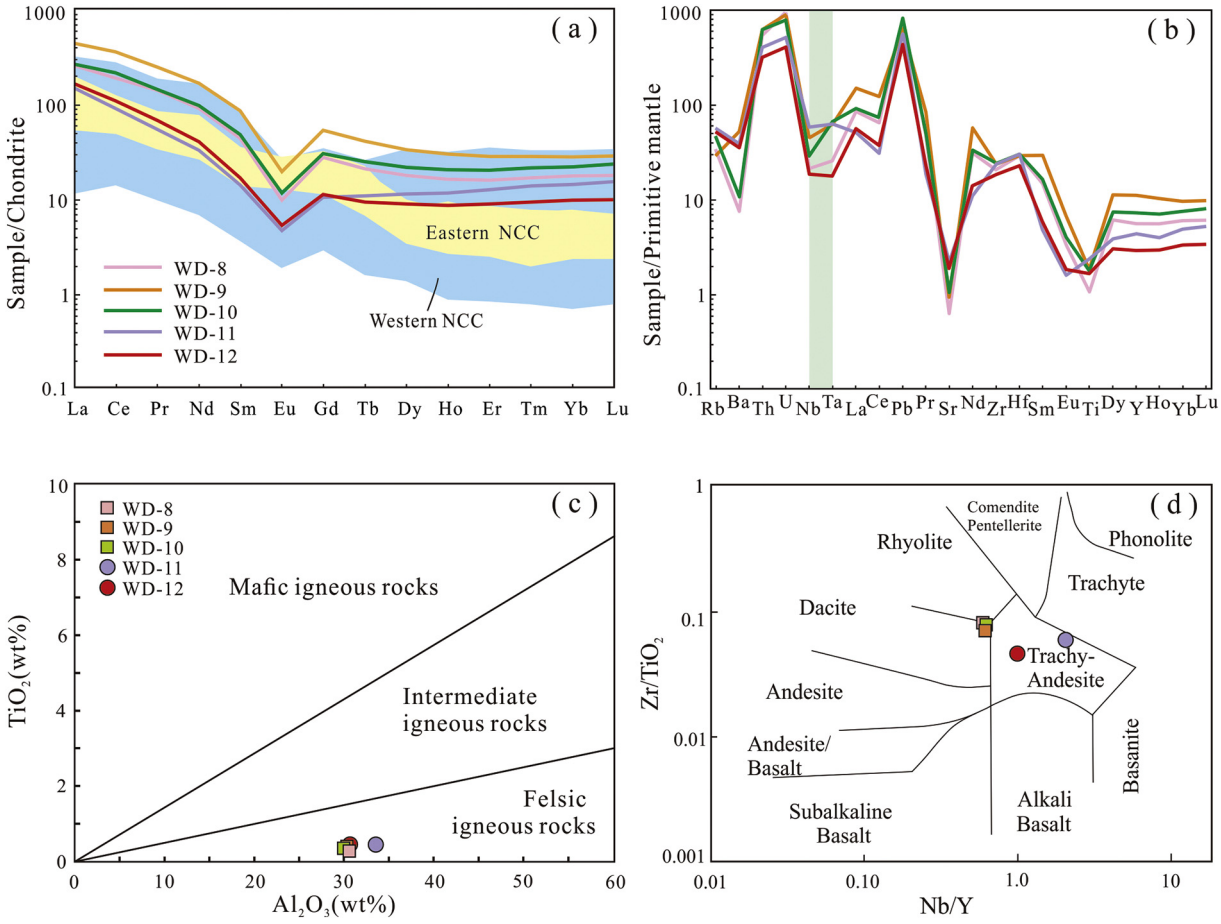

Fig. 3. (a) Diagram of chondrite-normalized REE patterns for the Wuda Tuff samples and contemporaneous pyroclastic rocks (Peng and Zhong, 1995; Zhao et al., 2019; Zhong et al., 1995, 1996; Zhou et al., 2001). (b) Primitive-mantle-normalized trace-element spider diagram. Normalization values are from Sun and McDonough (1989). (c) TiO_2–Al_2O_3 discrimination diagram for the Wuda Tuff samples (Spears and Kanaris-Sotiriou, 1979). (d) Nb/Y–Zr/TiO_2 classification diagram for the Wuda Tuff samples (Winchester and Floyd, 1977).

2003). Dating results for samples WD-9 and WD-10 are clustered mainly in the range of 317–286 Ma and show a distinct single age peak. Twenty-one zircon grains from WD-9 yield a weighted mean $^{206}Pb/^{238}U$ age of 295.7 ± 2.5 Ma (1σ, MSWD = 1.5, n = 21) (Fig. 5b). Nineteen zircon grains from WD-10 yield a weighted mean $^{206}Pb/^{238}U$ age of 296.7 ± 2.1 Ma (1σ, MSWD = 0.79, n = 19) (Fig. 5d). Pooling the data for zircons from the two samples yields a weighted mean $^{206}Pb/^{238}U$ age of 295.9 ± 1.4 Ma (1σ, MSWD = 0.94, n = 39) (Fig. 5e).

4.4. Zircon in situ Hf—O isotopic compositions

In situ Hf and O isotopic analyses were performed on the same zircons from samples WD-9 and WD-10 as used for U—Pb dating (Supplementary Table S3). Zircon grains from sample WD-9 have $\varepsilon_{Hf}(t)$ values of 0.0 to +5.0 and $\delta^{18}O$ values of 5.05‰ to 6.04‰. Zircon grains from sample WD-10 have $\varepsilon_{Hf}(t)$ values of +0.1 to +3.7 (except for a single negative value of −2.5) and $\delta^{18}O$ values of 5.56‰ to 6.17‰ (Fig. 6a, b).

5. Discussion

5.1. Wuda Tuff Flora: preservation in a felsic tuff bed

Our field observations indicate that the bed containing the Wuda Tuff Flora has the following typical features of a tuff: (1) lateral continuity over an area of about 20 km^2 (Pfefferkorn and Wang, 2007; Wang et al., 2013), (2) sharp contacts with the host coal seams, and (3) an absence of cross-bedding and sedimentary layering structures.

In addition, the mineral compositions and textures of samples from this bed are similar to those of typical altered tuffs in coal seams (Dai et al., 2017). Generally, diagenetic transformation of tuffs in coal seams involves kaolinite and original volcanogenic quartz, transforming

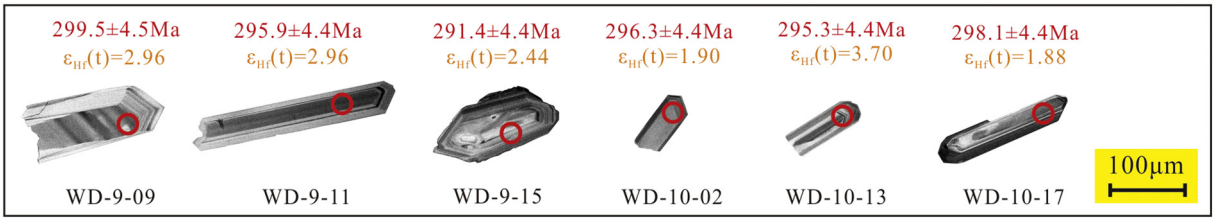

Fig. 4. Representative CL images of zircons from samples WD-9 and WD-10 of the Wuda Tuff.

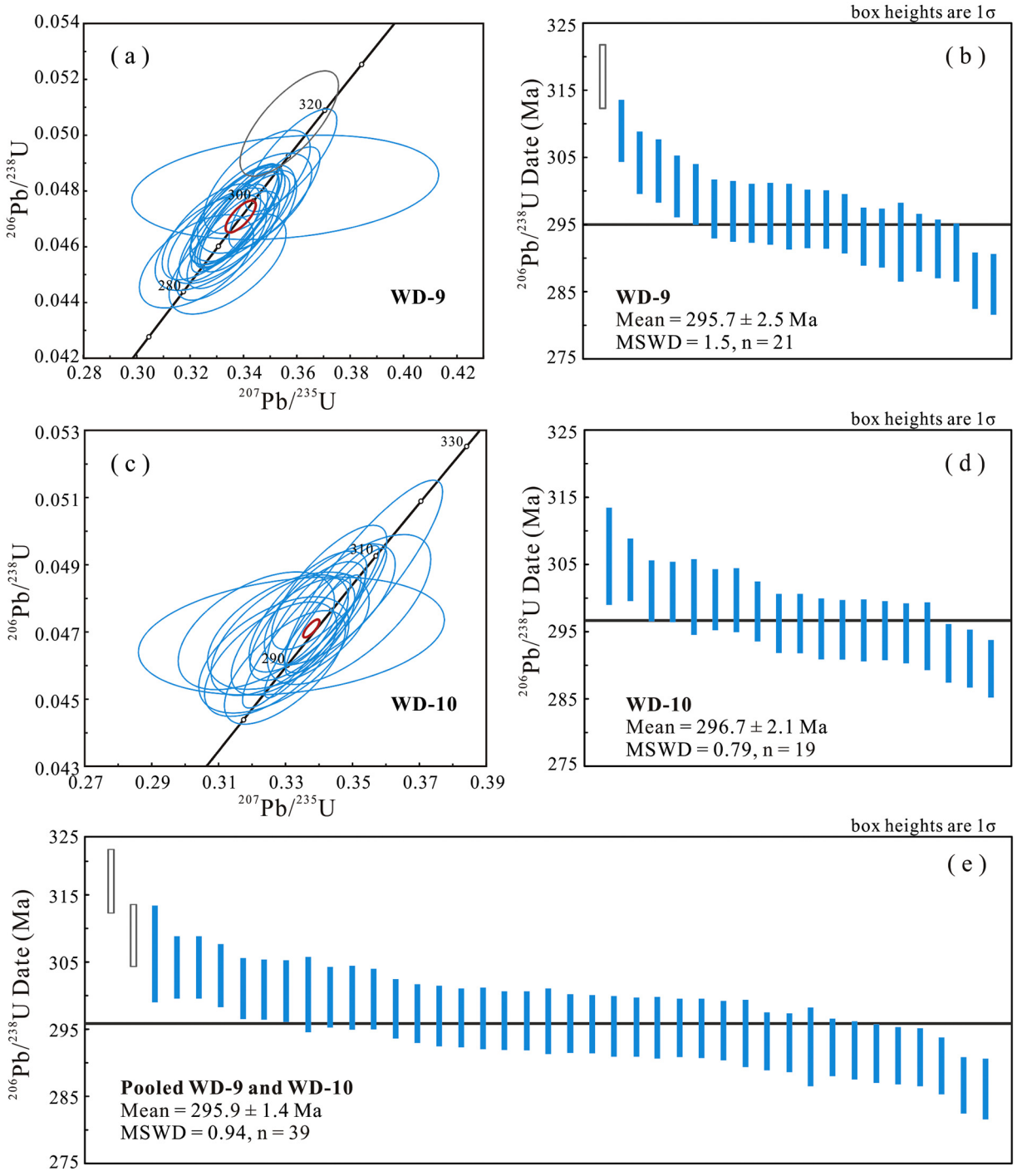

Fig. 5. (a and c) SIMS zircon U—Pb concordia diagrams for samples (a) WD-9 and (c) WD-10. (b, d, and e) Ranked-age plots for individual analyses yielding weighted mean $^{206}Pb/^{238}U$ ages for samples (b) WD-9, (d) WD-10, and (e) pooled WD-9 and WD-10.

the original feldspar crystals and volcanic glasses into kaolinite (Dai et al., 2017). In the present study, the Wuda samples have undergone intensive post-deposition alteration with high CIA ratios (96.7–98.1), dominated by kaolinite (74.3%–86.5%) that was altered from feldspar crystals (Fig. 2d) and volcanic glasses. Furthermore, quartz crystals in the Wuda samples retain the original shapes of pyroclastic materials, such as angular shapes and corrosion gulfs (Fig. 2b, c), indicating a volcanic origin.

The zircon U—Pb ages of the two analyzed samples display a single age peak, indicating that the sampled bed was formed during a very short time interval, in turn suggesting that a strong volcanic eruption produced a single thick tuff bed.

All of the above lines of evidence confirm that the bed hosting the Wuda Tuff Flora is an altered volcanic tuff. The geochemical results further support a felsic volcanic origin of the altered tuff. The Wuda samples plot within the felsic origin field in an TiO_2–Al_2O_3 discrimination diagram (Fig. 3c; Spears and Kanaris-Sotiriou, 1979). The samples have strong negative Eu anomalies that indicate a felsic magma origin through early Eu-enriched plagioclase crystallization and melt extraction. This explanation of negative Eu anomalies assumes that the altered

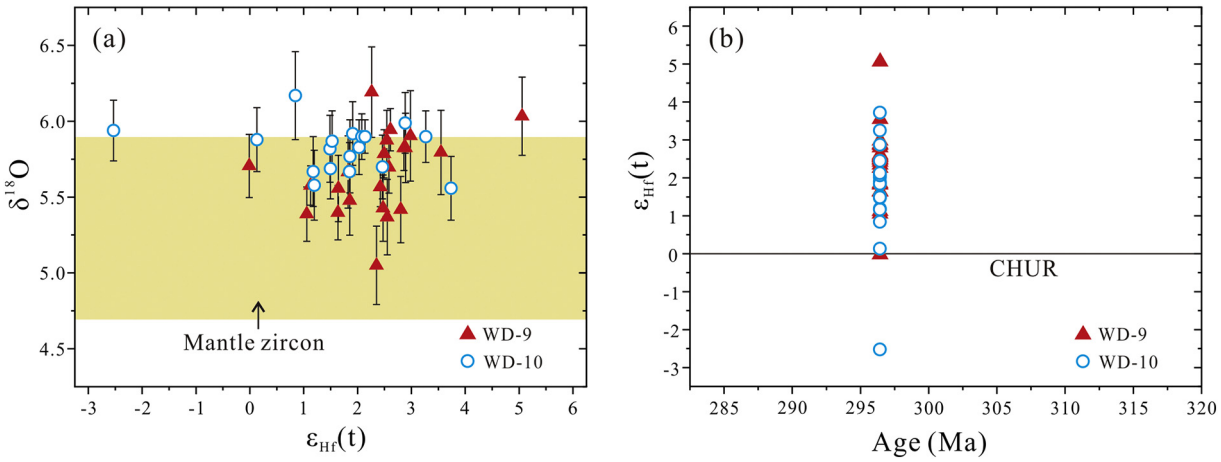

Fig. 6. Plots of (a) $\varepsilon_{Hf}(t)$ *versus* $\delta^{18}O$ for zircons from the Wuda Tuff. The gray field depicts the $\delta^{18}O$ values (mean of 5.3‰ ± 0.6‰, 2SD) of mantle-derived zircons (Valley et al., 1998), and (b) $\varepsilon_{Hf}(t)$ *versus* U—Pb age for zircons from the Wuda Tuff.

tuff was not subjected to post-deposition high-temperature hydrothermal alteration, as supported by zircon $\delta^{18}O$ values that are close to normal mantle zircon $\delta^{18}O$ values (Fig. 6a; Valley et al., 1998). In a Zr/TiO_2 *versus* Nb/Y diagram (Winchester and Floyd, 1977), the Wuda Tuff samples plot within the trachyandesite and rhyodacite–dacite fields rather than the rhyolite field (Fig. 3d). This distribution may be caused by the loss of Y owing to the loss of REE and Y carrier minerals when the upper and lower parts of the tuff layer reacted with the adjacent coal seams during weathering (Dai et al., 2016).

5.2. Age of the Wuda Tuff Flora

This study has provided the first SIMS U—Pb zircon age for the Wuda Tuff Flora. Although biostratigraphic correlations have been attempted, the age of the Wuda Tuff Flora has previously been uncertain. For example, Wang and Pfefferkorn (2013) suggested that the flora is latest Carboniferous or earliest Permian, whereas Sun and Deng (2003) proposed an age of late early Permian. Our U—Pb SIMS dating of zircons from two samples in different vertical positions in the tuff bed yielded similar ages, with a pooled weighted mean age of 295.9 ± 1.4 Ma, thereby constraining the age of the vegetational Pompeii to the earliest Permian (Asselian). Furthermore, our new dating results add a new tight age constraint to the developing chronostratigraphic chart of late Paleozoic terrestrial sediments in the NCC.

The Asselian age of the earliest Permian was a crucial time for global evolution of both flora and tectonism. At that time, the flora was evolving to adapt to the marked change to cold climatic conditions (Wang, 2010; Zhou, 2017). Based on the precise age for the Wuda Tuff obtained in the present study, the Wuda Flora can now be compared both regionally and globally. Regarding tectonic evolution, the early Permian was a crucial time of final supercontinent convergence and closure of the PAO (Buslov et al., 2004; Golonka and Ford, 2000; Xiao et al., 2003). These tectonic events generated strong volcanism along the surrounding plate boundaries, which erupted massive volumes of pyroclastic deposits. The Wuda Tuff layer was likely produced by this volcanism, and the precise age for this layer may help constrain the location and timing of tectonic–volcanic activity, which we discuss in section 5.4.

5.3. Formation mechanism of the Wuda Tuff Flora

Pfefferkorn and Wang (2007) proposed a simple model to explain the Wuda Tuff Flora whereby the living biocommunity was killed and buried by a volcanic ash-fall, thus preserving plants as fossils *in situ* in the tuff layer.

Our study provides new insights into the volcanic eruption and material related to the formation of the Wuda vegetational Pompeii, thereby refining the previous model. The volcanic eruption was felsic and likely to be plinian eruption characterized by explosive eruptions

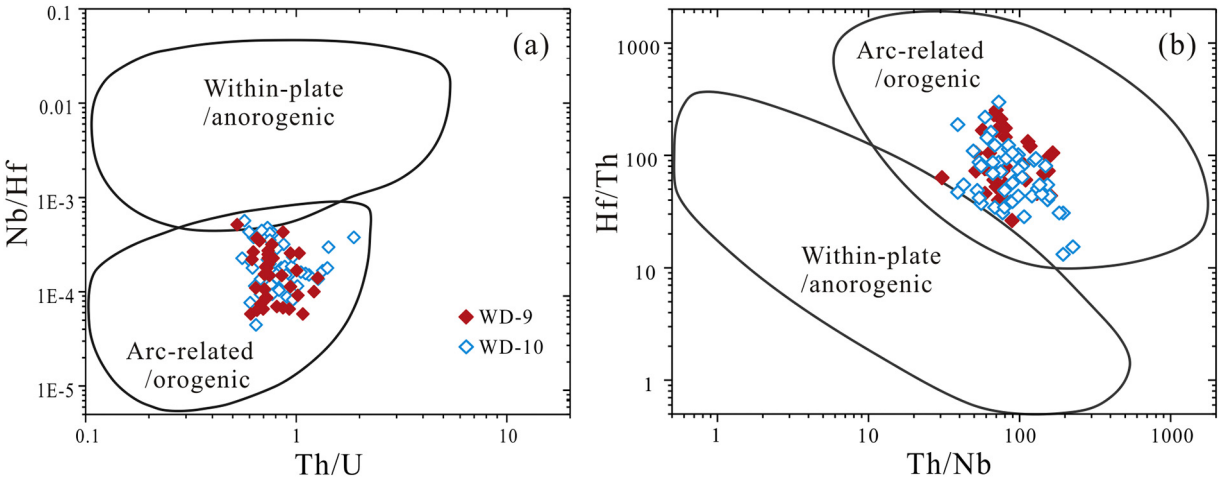

Fig. 7. (a) Th/U–Nb/Hf and (b) Th/Nb–Hf/Th diagrams for zircons from the Wuda Tuff. Modified after Yang et al. (2012).

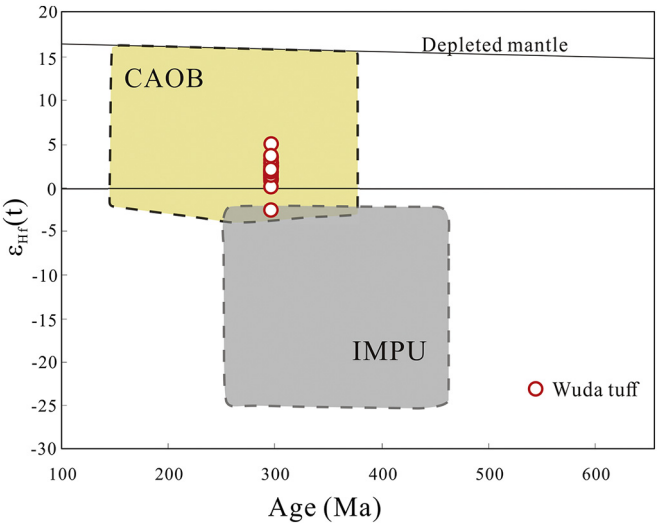

Fig. 8. Compilation diagram of $\varepsilon_{Hf}(t)$ *versus* U—Pb age for the Wuda Tuff, Central Asian Orogenic Belt (CAOB), and Inner Mongolia Paleo-Uplift (IMPU). Data are compiled from Li et al. (2010c), Su et al. (2012), Yang et al. (2006), Yuan and Yang (2015b), and Zhang et al. (2009a, 2009b).

with a high eruption column that rises massive volumes of volcanic ash to the stratosphere. Then, transported by airflows, this ash settled into the Wuda peat within days or weeks. The rapid deposition of volcanic ash killed the trees and buried the tree stumps *in situ*, with broken branches, having fallen, being positioned around the stumps. The burial processes of Wuda "vegetational Pompeii" is different from the Roman town Pompeii buried by volcano Vesuvius which was first covered by air-fall pumice and then buried by several Pyroclastic density currents (PDCs; Luongo et al., 2003). However, the Wuda "vegetational Pompeii" lacked the process of PDCs burial supported by the *in situ* preservation of fossils and unstratified Wuda Tuff layer. Furthermore, the ash-fall burial processes of Wuda "vegetational Pompeii" require larger volcanic eruption magnitude than volcano Vesuvius to rise and transport more volcanic ashes to distal places, maybe like the volcano Pinatubo's (Pyle, 2015).

After burial, the volcanic ash provided a particular taphonomic environment that favored fossilization. The thick and dense volcanic ash bed slowed decay processes by providing a low-bioturbation and anoxic environment (Rogers et al., 2001). The felsic volcanic ash bed was rich in SiO_2 and sulfate, which could have also favored fossilization processes during diagenesis (Luthardt et al., 2018).

5.4. Tectonic implications of the Wuda Tuff

The Wuda Tuff likely originated from volcanism in a magmatic arc setting because no intraplate magmatic activity has been reported in the NCC during the earliest Permian. Furthermore, the following geochemical features of the Wuda Tuff also support a magmatic arc origin and further indicate that the arc magma was derived from juvenile crust. (1) In discrimination diagrams of U, Hf, Th, and Nb, zircons of the Wuda Tuff plot in the field of an arc-related/orogenic setting (Fig. 7a, b; Pearce and Peate, 1995; Yang et al., 2012); and (2) the positive $\varepsilon_{Hf}(t)$ values (+0.11 to +5.15; Fig. 6b) and relatively low $\delta^{18}O$ values (5.05‰–6.17‰) of zircons from the Wuda altered tuff indicate a parental magma derived from the mantle or juvenile crust. However, melt derived from the mantle requires extensive differentiation to generate felsic magma (Annen et al., 2006), so the parental magma of the Wuda Tuff was more likely to have been derived from melting of juvenile crust. Considering the magmatic arc distribution around the location of Wuda during the early Permian, the IMPU at the northern margin of the NCC is a possible source (Zhang et al., 2007a), but can be disregarded on account of geochemical evidence. First, the positive $\varepsilon_{Hf}(t)$ values of zircon grains from the Wuda Tuff differ from the negative $\varepsilon_{Hf}(t)$ values from late Paleozoic arc granitic plutons in the IMPU (Fig. 8). Second, the origin of the pyroclastic rocks in the eastern NCC has been suggested to be the IMPU (Zhang et al., 2007b). However, the Wuda Tuff shows different geochemical features from those pyroclastic deposits in the eastern NCC, indicating different origins (Fig. 3c). In particular, the Wuda Tuff has distinct negative Eu anomalies, whereas pyroclastic rocks in the eastern NCC display weak negative Eu anomalies (Peng and Zhong, 1995; Zhao et al., 2019; Zhong et al., 1995, 1996; Zhou et al., 2001).

The Wuda Tuff has similar positive $\varepsilon_{Hf}(t)$ values to those of rocks from the magmatic arc in the CAOB (Fig. 8; Su et al., 2012). However, if the thick Wuda tuff bed, which was ~150 cm in origin (Wang et al., 2013), was erupted from a distant volcano in the CAOB, tuff beds with

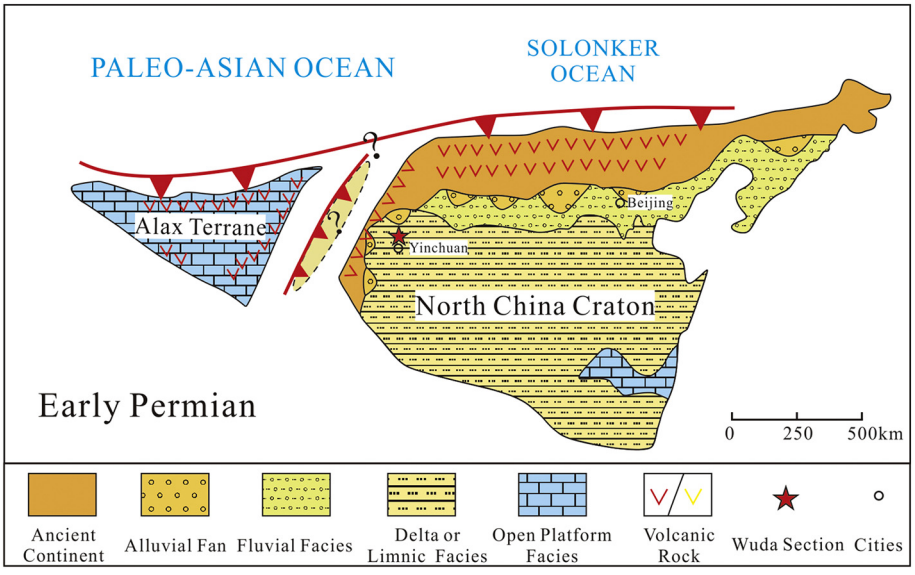

Fig. 9. Sketch paleogeographical map of the North China Craton and Alxa Terrane during the early Permian. The scale refers only to the sizes of terranes and locations of the Wuda section and city sites; the positions of terranes and magmatic arcs are not to scale. The lithofacies paleogeographic map is modified after Zhu et al. (2007).

positive Eu anomalies should be widely distributed in the NCC, which is inconsistent with the known distribution of tuff beds in the NCC. Therefore, the magmatic arc in the CAOB is unlikely to have been the source of the Wuda Tuff. Therefore, we consider that this tuff was erupted from a magmatic arc located along the western margin of the NCC, related to the subduction of PAO oceanic crust during the early Permian (Fig. 9). Although direct evidence for ophiolites related to the subduction is difficult to find because of strong deformation, evidence for a magmatic arc can be preserved by sedimentary records. Detrital zircons from the Early–Middle Jurassic Yan'an Formation in the Helan Mountain Range show an age peak from 305.2 ± 4.2 Ma to 271.0 ± 2.6 Ma (Zhao et al., 2015), which may record erosion and deposition of magmatic arc products during a time period encompassing the time of eruption of the Wuda Tuff.

An implication of the above hypothesis is that the ALT was separated from the NCC by a magmatic arc and a possible residual ocean. This possibility is important in terms of our understanding of the tectonic evolution of the CAOB, NCC and ALT. Therefore, the possible existence of a magmatic arc in this region around the earliest Permian needs to be verified by further work.

6. Conclusions

On the basis of petrographic, mineralogical, geochemical, zircon SIMS U—Pb geochronology, and *in situ* Hf—O isotopic analyses of the Wuda Tuff bed from the uppermost Taiyuan Formation in the western NCC, we are able to draw the following conclusions:

(1) The Wuda Tuff Flora was preserved in an altered felsic tuff bed, supporting a formation mechanism whereby the Wuda Flora was buried by a massive felsic ash-fall.
(2) Our zircon SIMS U—Pb dating of the tuff bed yielded a weighted mean age of 295.9 ± 1.4 Ma (1σ, MSWD = 0.94, $n = \underline{39}$). This provides the first precise constraint on the age of the Wuda Tuff Flora.
(3) The source of the Wuda Tuff was a volcano in a juvenile-crust-derived magmatic arc along the western margin of the NCC during the early Permian, implying that the ALT had not amalgamated with the NCC by that time.

Declaration of Competing Interest

The authors declare no conflict of interest. We declare that we have no financial or personal relationships with other people or organizations that can inappropriately influence the work submitted.

Acknowledgments

We thank Profs. Xuan-ce Wang, Yuan-bao Wu, Yan-hong Pan, and Dr. Wei-ming Zhou for advice and discussions. We are also grateful to Xiang-lin Tu, Jing-ming Wei, Xin-yu Wang, and Xiao-ping Xia for technical assistance. We acknowledge the constructive reviews and comments of Prof. Shi-feng Dai and an anonymous reviewer, and the Editor-in-Chief, Xian-hua Li. This research was funded by the Strategic Priority Research Program (B) of the Chinese Academy of Sciences (grant number XDB18000000) and the National Natural Science Foundation of China (grant number 41573028). This is contribution No.IS-2833 from GIGCAS.

Appendix A. Supplementary data

Supplementary data to this article can be found online at https://doi.org/10.1016/j.lithos.2020.105485.

References

Annen, C., Blundy, J.D., Sparks, R.S.J., 2006. The genesis of intermediate and silicic magmas in deep crustal hot zones. J. Petrol. 47, 505–539. https://doi.org/10.1093/petrology/egi084.

Buslov, M.M., Fujiwara, Y., Iwata, K., Semakov, N.N., 2004. Late paleozoic-early Mesozoic Geodynamics of Central Asia. Gondwana Res. 7, 791–808. https://doi.org/10.1016/s1342-937x(05)71064-9.

Dai, S.F., Ren, D.Y., Tang, Y.G., Shao, L.Y., Li, S.S., 2002. Distribution, isotopic variation and origin of sulfur in coals in the Wuda coalfield, Inner Mongolia, China. Int. J. Coal Geol. 51, 237–250. https://doi.org/10.1016/S0166-5162(02)00098-8.

Dai, S.F., Li, T.J., Jiang, Y.F., Ward, C.R., Hower, J.C., Sun, J.H., Liu, J.J., Song, H.J., Wei, J.P., Li, Q.Q., Xie, P.P., Huang, Q., 2015. Mineralogical and geochemical compositions of the Pennsylvanian coal in the Haishu Mine, Daqingshan Coalfield, Inner Mongolia, China: Implications of sediment-source region and acid hydrothermal solutions. Int. J. Coal Geol. 137, 92–110. https://doi.org/10.1016/j.coal.2014.11.010.

Dai, S.F., Graham, I.T., Ward, C.R., 2016. A review of anomalous rare earth elements and yttrium in coal. Int. J. Coal Geol. 159, 82–95. https://doi.org/10.1016/j.coal.2016.04.005.

Dai, S.F., Ward, C.R., Graham, I.T., French, D., Hower, J.C., Zhao, L., Wang, X., 2017. Altered volcanic ashes in coal and coal-bearing sequences: a review of their nature and significance. Earth-Sci. Rev. 175, 44–74. https://doi.org/10.1016/j.earscirev.2017.10.005.

Dan, W., Li, X.H., Wang, Q., Wang, X.C., Wyman, D.A., Liu, Y., 2016. Phanerozoic amalgamation of the Alxa Block and North China Craton: evidence from Paleozoic granitoids, U–Pb geochronology and Sr–Nd–Pb–Hf–O isotope geochemistry. Gondwana Res. 32, 105–121. https://doi.org/10.1016/j.gr.2015.02.011.

Darby, B.J., Ritts, B.D., 2002. Mesozoic contractional deformation in the middle of the Asian tectonic collage: the intraplate Western Ordos fold–thrust belt, China. Earth Planet. Sci. Lett. 205, 13–24. https://doi.org/10.1016/S0012-821X(02)01026-9.

Golonka, J., Ford, D., 2000. Pangean (late Carboniferous–Middle Jurassic) paleoenvironment and lithofacies. Palaeogeogr. Palaeoclimatol. Palaeoecol. 161, 1–34. https://doi.org/10.1016/s0031-0182(00)00115-2.

Goto, A., Tatsumi, Y., 1996. Quantitative analysis of rock samples by an X-ray fluorescence spectrometer (II). Rigaku J. 13, 20–39.

He, X.Z., Wang, S.J., Wang, J., 2016. *Chansitheca wudaensis* (Gleicheniaceae, fern) from the early Permian Wuda Tuff Flora, Inner Mongolia. Palaeoworld 25 (2), 199–211. https://doi.org/10.1016/j.palwor.2015.05.011.

Hou, Y.L., Zhong, Y.T., Xu, Y.G., He, B., 2017. The provenance of late Permian karstic bauxite deposits in SW China, constrained by the geochemistry of interbedded clastic rocks, and U–Pb–Hf–O isotopes of detrital zircons. Lithos 278–281, 240–254. https://doi.org/10.1016/j.lithos.2017.01.013.

Hower, J.C., Ruppert, L.F., Eble, C.F., 1999. Lanthanide, yttrium, and zirconium anomalies in the Fire Clay coal bed, Eastern Kentucky. Int. J. Coal Geol. 39, 141–153. https://doi.org/10.1016/S0166-5162(98)00043-3.

Li, J.Y., 2006. Permian geodynamic setting of Northeast China and adjacent regions: closure of the Paleo-Asian Ocean and subduction of the Paleo-Pacific Plate. J. Asian Earth Sci. 26, 207–224. https://doi.org/10.1016/j.jseaes.2005.09.001.

Li, X.H., Sun, M., Wei, G.J., Liu, Y., Lee, C.Y., Malpas, J., 2000. Geochemical and Sm-Nd isotopic study of amphibolites in the Cathaysia Block, southeastern China: evidence for an extremely depleted mantle in the Paleoproterozoic. Precambrian Res. 102, 251–262. https://doi.org/10.1016/S0301-9268(00)00067-X.

Li, X.H., Qi, C.S., Liu, Y., Liang, X.R., Tu, X.L., Xie, L.W., Yang, Y.H., 2005. Petrogenesis of the Neoproterozoic bimodal volcanic rocks along the western margin of the Yangtze Block: New constraints from Hf isotopes and Fe/Mn ratios. Chin. Sci. Bull. 50, 2481–2486. https://doi.org/10.1360/982005-287.

Li, X.H., Liu, Y., Li, Q.L., Guo, C.H., Chamberlain, K.R., 2009. Precise determination of Phanerozoic zircon Pb/Pb age by multicollector SIMS without external standardization. Geochem. Geophys. Geosyst. 10. https://doi.org/10.1029/2009GC002400.

Li, X.H., Li, W.X., Li, Q.L., Wang, X.C., Liu, Y., Yang, Y.H., 2010a. Petrogenesis and tectonic significance of the similar to 850 Ma Gangbian alkaline complex in South China: evidence from in situ zircon U-Pb dating, Hf-O isotopes and whole-rock geochemistry. Lithos 114, 1–15. https://doi.org/10.1016/j.lithos.2009.07.011.

Li, X.H., Long, W.G., Li, Q.L., Liu, Y., Zheng, Y.F., Yang, Y.H., Chamberlain, K.R., Wan, D.F., Guo, C.H., Wang, X.C., Tao, H., 2010b. Penglai Zircon Megacrysts: a potential new working reference material for microbeam determination of Hf-O isotopes and U-Pb age. Geostand. Geoanal. Res. 34, 117–134. https://doi.org/10.1111/j.1751-908X.2010.00036.x.

Li, H.Y., He, B., Xu, Y.G., Huang, X.L., 2010c. U–Pb and Hf isotope analyses of detrital zircons from late Paleozoic sediments: Insights into interactions of the North China Craton with surrounding plates. J. Asian Earth Sci. 39, 335–346. https://doi.org/10.1016/j.jseaes.2010.05.002.

Li, X.H., Tang, G.Q., Gong, B., Yang, Y.H., Hou, K.J., Hu, Z.C., Li, Q.L., Liu, Y., Li, W.X., 2013. Qinghu zircon: a working reference for microbeam analysis of U-Pb age and Hf and O isotopes. Chin. Sci. Bull. 58, 4647–4654. https://doi.org/10.1007/s11434-013-5932-x.

Li, D.D., Wang, J., Wan, S., Pšenička, J., Zhou, W.M., Jiří, B., Votočková-Frojdová, J., 2019. A marattialean fern, *Scolecopteris libera* n. sp., from the Asselian (Permian) of Inner Mongolia, China. Palaeoworld 28, 487–507. https://doi.org/10.1016/j.palwor.2019.05.002.

Liu, G.H., 1990. Permo-Carboniferous paleography and coal accumulation and their tectonic control in North China and South China continental plates. Int. J. Coal Geol. 16, 73–117. https://doi.org/10.1016/0166-5162(90)90014-P.

Liu, Y.S., Hu, Z.C., Gao, S., Guenther, D., Xu, J., Gao, C.G., Chen, H.H., 2008. In situ analysis of major and trace elements of anhydrous minerals by LA-ICP-MS without applying an internal standard. Chem. Geol. 257, 34–43. https://doi.org/10.1016/j.chemgeo.2008.08.004.

Ludwig, K., 2003. User's Manual for ISOPLOT 3.00: A Geochronological Toolkit for Microsoft Excel.
Luongo, G., Perrotta, A., Scarpati, C., 2003. Impact of the AD 79 eruption on Pompeii, I. Relations amongst the depositional mechanisms of the pyroclast products, the framework of the buildings and the associated destructive events. J. Volcanol. Geotherm. Res. 126, 201–223. https://doi.org/10.1016/S0377-0273(03)00146-X.
Luthardt, L., Hofmann, M., Linnemann, U., Gerdes, A., Marko, L., Rößler, R., 2018. A new U–Pb zircon age and a volcanogenic model for the early Permian Chemnitz Fossil Forest. Int. J. Earth Sci. 107, 2465–2489. https://doi.org/10.1007/s00531-018-1608-8.
Nesbitt, H.W., Young, G.M., 1982. Early Proterozoic climates and plate motions inferred from major chemistry of lutites. Nature 299, 19–40. https://doi.org/10.1038/299715a0.
Pearce, J.A., Peate, D.W., 1995. Tectonic implications of the composition of volcanic arc magmas. Annu. Rev. Earth Planet. Sci. 23, 251–285. https://doi.org/10.1146/annurev.earth.23.1.251.
Peng, G.L., Zhong, R., 1995. Discovery of volcanic event deposits and stratigrafic correlation of Taiyuan Formation in western margin of North China. Geoscience 9 (1), 108–119 (in Chinese with English abstract).
Pfefferkorn, H.W., Wang, J., 2007. Early Permian coal-forming floras preserved as compressions from the Wuda District (Inner Mongolia, China). Int. J. Coal Geol. 69, 90–102. https://doi.org/10.1016/j.coal.2006.04.012.
Pyle, D.M., 2015. Sizes of volcanic eruptions. The Encyclopedia of Volcanoes. Academic Press, pp. 257–264. https://doi.org/10.1016/B978-0-12-385938-9.00013-4.
Rogers, R.R., Arcucci, A.B., Abdala, F., Sereno, P.C., Forster, C.A., May, C.L., 2001. Paleoenvironment and taphonomy of the Chañares Formation tetrapod assemblage (Middle Triassic), northwestern Argentina: spectacular preservation in volcanogenic concretions. Palaios 16, 461–481. https://doi.org/10.1669/0883-1351(2001)016<0461:PATOTC>2.0.CO;2.
Slama, J., Kosler, J., Condon, D.J., Crowley, J.L., Gerdes, A., Hanchar, J.M., Horstwood, M.S.A., Morris, G.A., Nasdala, L., Norberg, N., Schaltegger, U., Schoene, B., Tubrett, M.N., Whitehouse, M.J., 2008. Plesovice zircon - a new natural reference material for U-Pb and Hf isotopic microanalysis. Chem. Geol. 249, 1–35. https://doi.org/10.1016/j.chemgeo.2007.11.005.
Spears, D.A., Kanaris-Sotiriou, R., 1979. A geochemical and mineralogical investigation of some British and other European tonsteins. Sedimentology 26, 407–425. https://doi.org/10.1111/j.1365-3091.1979.tb00917.x.
Su, B.X., Qin, K.Z., Sun, H., Tang, D.M., Sakyi, P.A., Chu, Z.Y., Liu, P.P., Xiao, Q.H., 2012. Subduction-induced mantle heterogeneity beneath Eastern Tianshan and Beishan: Insights from Nd–Sr–Hf–O isotopic mapping of late Paleozoic mafic–ultramafic complexes. Lithos 134–135, 41–51. https://doi.org/10.1016/j.lithos.2011.12.011.
Sun, K.Q., Deng, S.H., 2003. Carboniferous and Permian flora in the northern part of the Helan Mountains. Geoscience 17, 259–267 (in Chinese with English abstract). https://doi.org/10.1016/S0955-2219(02)00073-0.
Sun, S.S., McDonough, W.F., 1989. Chemical and isotopic systematics of oceanic basalts: implications for mantle composition and processes. Geol. Soc. Lond. Spec. Publ. 42 (1), 313–345. https://doi.org/10.1144/GSL.SP.1989.042.01.19.
Sun, K.Q., Zhang, Z.L., Chen, C.L., 1998. Early early Permian flora in Wuda Area of Inner Mongolia. Geoscience 12 (4), 586–590 (in Chinese with English abstract).
Valley, J.W., Kinny, P.D., Schulze, D.J., Spicuzza, M.J., 1998. Zircon megacrysts from kimberlite: oxygen isotope variability among mantle melts. Contrib. Mineral. Petrol. 133, 1–11. https://doi.org/10.1007/s004100050432.
Wang, J., 2010. Late Paleozoic macrofloral assemblages from Weibei Coalfield, with reference to vegetational change through the late Paleozoic Ice-age in the North China Block. Int. J. Coal Geol. 83, 292–317. https://doi.org/10.1016/j.coal.2009.10.007.
Wang, J., Pfefferkorn, H.W., 2013. The Carboniferous-Permian transition on the North China microcontinent - Oceanic climate in the tropics. Int. J. Coal Geol. 119, 106–113. https://doi.org/10.1016/j.coal.2013.07.022.
Wang, J., Pfefferkorn, H.W., Jiří, B., 2009. *Paratingia wudensis* sp. nov., a whole noeggerathialean plant preserved in an air fall tuff of earliest Permian age (Inner Mongolia, China). Am. J. Bot. 96 (9), 1676–1689. https://doi.org/10.3732/ajb.0800351.
Wang, J., Pfefferkorn, H.W., Zhang, Y., Feng, Z., 2012. Permian vegetational Pompeii from Inner Mongolia and its implications for landscape paleoecology and paleobiogeography of Cathaysia. Proc. Natl. Acad. Sci. https://doi.org/10.1073/pnas.1115076109.
Wang, J., He, X.Z., Pfefferkorn, H.W., Wang, J.R., 2013. Compaction Rate of an early Permian Volcanic Tuff from Wuda Coalfield, Inner Mongolia. Acta Geol. Sin. Engl. Ed. 87, 1242–1249. https://doi.org/10.1111/1755-6724.12125.
Wang, J., Wan, M.L., Pfefferkorn, H.W., 2014a. Aphlebia hvistendahliae sp. nov. from the early Permian Wuda Tuff Flora, Inner Mongolia. Rev. Palaeobot. Palynol. 210, 69–76. https://doi.org/10.1016/j.revpalbo.2014.08.001.
Wang, J., Pfefferkorn, H.W., Feng, Z., 2014b. Noeggerathiales as coal-forming plants in Cathaysia: conclusions from an early Permian vegetational Pompeii in Inner Mongolia. Chin. Sci. Bull. 59 (23), 2785–2792. https://doi.org/10.1007/s11434-014-0270-1.
Wang, Q.F., Deng, J., Liu, X.F., Zhao, R., Cai, S.H., 2016. Provenance of late Carboniferous bauxite deposits in the North China Craton: New constraints on marginal arc construction and accretion processes. Gondwana Res. 38, 86–98. https://doi.org/10.1016/j.gr.2015.10.015.
Whitehouse, M.J., Claesson, S., Sunde, T., Vestin, J., 1997. Ion microprobe U-Pb zircon geochronology and correlation of Archaean gneisses from the Lewisian complex of Gruinard Bay, northwestern Scotland. Geochem. Cosmochim. Acta 61, 4429–4438. https://doi.org/10.1016/S0016-7037(97)00251-2.
Winchester, J.A., Floyd, P.A., 1977. Geochemical discrimination of different magma series and their differentiation products using immobile elements. Chem. Geol. 20, 325–343. https://doi.org/10.1016/0009-2541(77)90057-2.
Xiao, W.J., Windley, B.F., Hao, J., Zhai, M.G., 2003. Accretion leading to collision and the Permian Solonker suture, Inner Mongolia, China: termination of the central Asian orogenic belt. Tectonics 22. https://doi.org/10.1029/2002TC001484.
Yan, M.X., Milan, L., Jiří, B., Wang, J., 2013. Morphological reconstruction and ecological habit of *Sphenophyllum angustifolium* (Germar) Goeppert from early Permian of Wuda, Inner Mongolia. Acta Palaeontol. Sin. 52 (4), 467–483 (in Chinese with English abstract). 10.19800/j.cnki.aps.2013.04.005.
Yang, J.H., Wu, F.Y., Shao, J.A., Wilde, S.A., Xie, L.W., Liu, X.M., 2006. Constraints on the timing of uplift of the Yanshan Fold and Thrust Belt, North China. Earth Planet. Sci. Lett. 246, 336–352. https://doi.org/10.1016/j.epsl.2006.04.029.
Yang, J.H., Cawood, P.A., Du, Y.S., Huang, H., Huang, H.W., Tao, P., 2012. Large Igneous Province and magmatic arc sourced Permian-Triassic volcanogenic sediments in China. Sediment. Geol. 261, 120–131. https://doi.org/10.1016/j.sedgeo.2012.03.018.
Yuan, W., Yang, Z.Y., 2015a. The Alashan Terrane did not amalgamate with North China block by the late Permian: evidence from Carboniferous and Permian paleomagnetic results. J. Asian Earth Sci. 104, 145–159. https://doi.org/10.1016/j.jseaes.2014.02.010.
Yuan, W., Yang, Z.Y., 2015b. The Alashan Terrane was not part of North China by the late Devonian: evidence from detrital zircon U–Pb geochronology and Hf isotopes. Gondwana Res. 27, 1270–1282. https://doi.org/10.1016/j.gr.2013.12.009.
Zhang, S.H., Zhao, Y., Song, B., Yang, Z.Y., Hu, J.M., Wu, H., 2007a. Carboniferous granitic plutons from the northern margin of the North China block: implications for a late Palaeozoic active continental margin. J. Geol. Soc. Lond. 164, 451–463. https://doi.org/10.1144/0016-76492005-190.
Zhang, S.H., Zhao, Y., Song, B., Yang, Y.H., 2007b. Zircon SHRIMP U-Pb and in-situ Lu-Hf isotope analyses of a tuff from Western Beijing: evidence for missing late Paleozoic arc volcano eruptions at the northern margin of the North China block. Gondwana Res. 12, 157–165. https://doi.org/10.1016/j.gr.2006.08.001.
Zhang, S.H., Zhao, Y., Kroener, A., Liu, X.M., Xie, L.W., Chen, F.K., 2009a. Early Permian plutons from the northern North China Block: constraints on continental arc evolution and convergent margin magmatism related to the Central Asian Orogenic Belt. Int. J. Earth Sci. 98, 1441–1467. https://doi.org/10.1007/s00531-008-0368-2.
Zhang, S.H., Zhao, Y., Song, B., Hu, J.M., Liu, S.W., Yang, Y.H., Chen, F.K., Liu, X.M., Liu, J., 2009b. Contrasting late Carboniferous and late Permian-Middle Triassic intrusive suites from the northern margin of the North China craton: Geochronology, petrogenesis, and tectonic implications. Geol. Soc. Am. Bull. 121, 181–200. https://doi.org/10.1130/B26157.1.
Zhang, J., Li, J., Xiao, W.X., Wang, Y.N., Qi, W.H., 2013. Kinematics and geochronology of multistage ductile deformation along the eastern Alxa block, NW China: New constraints on the relationship between the North China Plate and the Alxa block. J. Struct. Geol. 57, 38–57. https://doi.org/10.1016/j.jsg.2013.10.002.
Zhang, L., Ren, Z.Y., Nichols, A.R.L., Zhang, Y.H., Zhang, Y., Qian, S.P., Liu, J.Q., 2014. Lead isotope analysis of melt inclusions by LA-MC-ICP-MS. J. Anal. At. Spectrom. 29, 1393–1405. https://doi.org/10.1039/c4ja00088a.
Zhang, L., Ren, Z.Y., Xia, X.P., Li, J., Zhang, Z.F., 2015. IsotopeMaker: a Matlab program for isotopic data reduction. Int. J. Mass Spectrom. 392, 118–124. https://doi.org/10.1016/j.ijms.2015.09.019.
Zhao, H.G., Liu, C.Y., Wang, H.R., Gao, S.H., Li, M., Zhuo, Y.Z., Qiao, J.X., Zhang-Sun, X.Q., Jiang, S., 2015. LA-ICP-MS detrital zircon dating and its provenance significance in Yan'an Formation of the Early-Middle Jurassic in the northwestern margin of Ordos Basin. Earth Sci. Front. 22 (3), 184–193 (in Chinese with English abstract). 10.13745/j.esf.2015.03.016.
Zhao, L., et al., 2019. Enrichment of critical elements (Nb-Ta-Zr-Hf-REE) within coal and host rocks from the Datanhao mine, Daqingshan Coalfield, northern China. Ore Geol. Rev. 111, 102951. https://doi.org/10.1016/j.oregeorev.2019.102951.
Zhong, R., Sun, S.P., Chen, F., Fu, Z.M., 1995. The discovery of rhyo-tuffite in the Taiyuan Formation and stratigraphic correlation of the Daqingshan and Datong coalfields. Acta Geosci. Sin. 3, 291–301 (in Chinese with English abstract).
Zhong, R., Sun, S.P., Fu, Z.M., 1996. The Characteristics of volcanic event deposits and their temporal-spatial distribution of Benxi and Taiyuan Formations in North China Platform (NCP). J. Geom. 2 (1), 83–91 (in Chinese with English abstract).
Zhou, F., 2017. Late Palaeozoic plants. Curr. Biol. 27, R905–R909. https://doi.org/10.1016/j.cub.2017.07.041.
Zhou, A.C., Jia, B.W., Ma, M.L., Zhang, H., 2001. The whole sequences of volcanic event deposits on the north margin of the North China Plate and their features. Geol. Rev. 47, 175–184 (in Chinese with English abstract). 10.16509/j.georeview.2001.02.011.
Zhou, W.M., Li, D.D., Pšenička, J., Boyce, C.K., Wang, J., 2019. A left-handed fern twiner in a Permian swamp forest. Curr. Biol. 29, 1172–1173. https://doi.org/10.1016/j.cub.2019.10.005.
Zhu, R.K., Xu, H.X., Deng, S.H., Guo, H.L., 2007. Lithofacies palaeogeography of the Permian in northern China. J. Palaeogeogr. 9 (2), 133–142 (in Chinese with English abstract).